Biomedical Signal Processing and Control 60 (2020) 101943

Contents lists available at ScienceDirect

Biomedical Signal Processing and Control

journal homepage: www.elsevier.com/locate/bspc

Combining MF-DFA and LSSVM for retina images classification

Jian Wang [a], Wei Shao [b], Junseok Kim [c,*]

[a] School of Mathematics and Statistics, Nanjing University of Information Science and Technology, Nanjing, 210044, China
[b] Department of Economics, Korea University, Seoul 02841, Republic of Korea
[c] Department of Mathematics, Korea University, Seoul 02841, Republic of Korea

ARTICLE INFO

Article history:
Received 8 October 2019
Received in revised form 22 February 2020
Accepted 28 March 2020
Available online 15 May 2020

Keywords:
Multifractal
Retina
Least square support vector machine
Classification

ABSTRACT

Diabetic retinopathy is the main cause of blindness in adults. Early diagnosis of diabetic retinopathy is essential for avoiding deterioration of illness and vision loss. The use of computer technology to identify diabetic retinopathy images provides significant means to reduce the risk of deterioration. In this paper, we propose a new approach for retina images detection and classification by using a hybrid system which is constructed by two-dimensional multifractal detrended fluctuation analysis (2D MF-DFA) and least square support vector machines (LSSVM). In the proposed method, we applied 2D MF-DFA to compute the local generalized Hurst exponents which are the multifractal features of the diabetic retinopathy image, and these values are recorded as LH_q. Then, the Hurst exponents are taken as the training input vector for the training in LSSVM. Finally, we classified a specific retina image as healthy or lesion image. We present experimental verification to investigate the efficiency and robustness of the proposed system. The results show that the proposed system yields a classification accuracy with 99.01% ± 0.0074, sensitivity with 99.03% ± 0.0051, and specificity with 97.73% ± 0.0075. When the performance was compared with state-of-the-arts, the solution indicated that the MF-DFA-LSSVM system outperforms most of others in terms of all the classification sensitivity, accuracy, and specificity. The proposed method will be useful for clinical medicine.

1. Introduction

Diabetic retinopathy is a frequent complication of diabetes mellitus, and is one of the most significant causes of vision loss worldwide [1]. In the recent years, studies of human retina images classification of healthy and diabetic retinopathy images have produced great impacts on research and clinic. In Thakur's survey [2], the authors summarized the segmentation methods of optic disc and cup by different researchers and their classification in the diagnosis of glaucoma. A review for registration techniques and automated detection methods for diabetic retinopathy color fundus images was also conducted in [3]. In the classification of retinal pathological images, the extraction of the representative and discriminatory features was the key factor to achieve good classification results. The manual classification of retinal images has some problems, such as it is difficult to extract discriminant features, poor classification performance, time-consuming and laborious, and difficult to obtain objective and unified medical diagnosis.

Therefore, how to design a more intelligent retinal image analysis system is an urgent need. In the recent years, machine learning technology has attracted wide attention. In human retina images classification, according to the spectral and spatial information, each pixel in an image is assigned with a unique label, and various machine learning algorithms have been proposed for the classification. In Acharya's work [4], the authors used a sample consisting of 510 healthy and glaucoma images. Gabor transformation and principal component analysis were used to extract the features in these images, then ranked the features. Finally, a support vector machine classifier was used for classifying the images. High accuracy, sensitivity and specificity were achieved in their study. By using support vector machine classifier, Raghavendra proposed a hybrid system and yielded a maximum accuracy with 97.00%, sensitivity with 97.80%, and specificity with 95.80% [5]. In [6], the least squares support vector machine was used to classify the retina images by the features obtained from variational mode decomposition method. By using 3-fold and 10-fold cross-validation methods, the proposed algorithm produced classification accuracies of 95.19% and 94.79%. Moreover, a diabetic retinal image classification system based on deep neural network has also been widely used in the recent years. A deep learning system for the classification of glaucomatous optic neuropathy was developed for automated classification of glauco-

* Corresponding author.
E-mail addresses: super_wj150@163.com (J. Wang), cfdkim@korea.ac.kr (J. Kim).
URL: http://math.korea.ac.kr/~cfdkim/ (J. Wang).

https://doi.org/10.1016/j.bspc.2020.101943
1746-8094/

matous optic neuropathy on color fundus photographs in [7]. In their validation, the system achieved an accuracy, sensitivity, and specificity of 98.6%, 95.6%, and 92.0%, respectively. Convolutional neural network (CNN) is a standard multi-layer neural network structure composed of convolution, pooling, and full connection layers. Convolutional neural networks can learn some simple local features from images, such as curves, textures, and other information; and these local features can be combined into complex local or global features to restore objects in order to achieve image recognition and classification. An eighteen layer CNN framework was developed for glaucoma diagnosis in [8]. By using 589 healthy and 837 glaucoma fundus images, the authors attained a high accuracy of 98.13%.

MF-DFA has recently been used to describe complex non-linear systems [9]. The 1D MF-DFA was widely applied to the time series in many fields [10–13]. As a meaningful expansion, Gu et al. [14] used the 2D MF-DFA to analyze multifractal surfaces. Since then, the 2D MF-DFA has been used for some studies to implement for some specific image analysis [15]. The 2D MF-DFA is performed by the local Hurst exponent LH_q, quality indexes $\tau(q)$, and multifractal spectrum $\Delta\alpha$, which can analyze the scaling properties of images. Although many methods have been proposed to classify the images with healthy and unhealthy human retina images, the combination of the 2D MF-DFA model and LSSVM has hardly been applied to the research of lesion retina images. In this article, we combined 2D MF-DFA and LSSVM for retina images classification. The proposed ensemble classifier MF-DFA-LSSVM does not need predetermined regions of interests or manually-determined, which is different from the previous methods [6,16–18].

In Section 2, we introduce the MF-DFA, LSSVM, and leave-one-out cross-validation methods. In Section 3, we provide data collection. In Section 4, we conduct empirical experiments and provide classification results. Section 5 is the discussion section. In Section 6, some conclusions are delivered.

2. Principles and methodology

In this section, we will provide a description of the methods used in this paper. 2D MF-DFA, LSSVM, and leave-one-out cross-validation (LOOCV) method were utilized for the research. We used 2D MF-DFA to compute the local generalized Hurst exponent LH_q of a given retina image. Then, the multifractal exponents were taken as the training set for the LSSVM. In the process of classification, the leave-one-out cross-validation method was applied. Next, we classified a specific retina image as healthy or lesion image. Finally, to evaluate the performance of the proposed model, we used three metrics such as the accuracy, sensitivity, and specificity. In Fig. 1, the classification process of our hybrid system is shown.

2.1. 2D MF-DFA

The 2D MF-DFA method and procedure can be conducted as follows: (i) Consider a two-dimensional image, which can be discretized into an $M \times N$ matrix $X_{i,j}$, where $i = 1, 2, \ldots, M$, and $j = 1, 2, \ldots, N$. We first divide the image into non-overlapping sub-regions of equal length s, the size of which is $M_s \times N_s$, and each sub-region is defined as $X_{m,n}(i,j) = X((m-1)s+i, (n-1)s+j)$ for $1 \le i, j \le s$. Here, $M_s = M/s$ and $N_s = N/s$. The cumulative sum $U_{m,n}(i,j)$ of surface pixels for each sub-region is:

$$U_{m,n}(i,j) = \sum_{k_1=1}^{i}\sum_{k_2=1}^{j} X_{m,n}(k_1, k_2). \tag{1}$$

(ii) Then, we used the plane $\overline{U}_{m,n}(i,j)$ to fit the trend of $U_{m,n}(i,j)$ in each sub-region. We noted that $U_{m,n}(i,j)$ is a surface, according to [14,15,19], a simple function $\overline{U}_{m,n}(i,j) = ai + bj + c$ can be taken to get the fitting polynomial with k-order by 1 for i and j, in each region by using the least squares method. Define the element $u_{m,n}(i, j)$ in residual matrix:

$$u_{m,n}(i,j) = U_{m,n}(i,j) - \overline{U}_{m,n}(i,j). \tag{2}$$

(iii) The detrended fluctuation function $F^2(m, n, s)$ of each sub-region can be obtained by residual matrix, which is defined as follows:

$$F^2(m,n,s) = \frac{1}{s^2}\sum_{i=1}^{s}\sum_{j=1}^{s}(u_{m,n}(i,j))^2. \tag{3}$$

According to the detrended fluctuation function of each sub-region, the qth-order wave function for each sub-region was calculated as

$$F_q(s) = \left\{\frac{1}{M_s N_s}\sum_{m=1}^{M_s}\sum_{n=1}^{N_s}[F(m,n,s)]^q\right\}^{\frac{1}{q}}. \tag{4}$$

When $q = 0$, according to Lopida's law,

$$F_q(s) = \exp\left(\frac{1}{M_s N_s}\sum_{m=1}^{M_s}\sum_{n=1}^{N_s}\ln[F(m,n,s)]\right). \tag{5}$$

(iv) Finally, by varying the range of s, a set of power relations between fluctuation functions $F_q(s)$ and scales s were obtained as follows:

$$F_q(s) \propto s^{h(q)}, \tag{6}$$

where $h(q)$ is the generalized Hurst exponent, $h(q)$ describes the image features, and it extracts different regions according to different values of $h(q)$, then segments the image and obtains the image features of each pixel. It is performed at each pixel (i, j), by using a $v \times v$ moving window centered at (i, j). We can then calculate $h(q)$ for this window and consider it as the property of the pixel (i, j). This is called local $h(q)$, which is expressed as $L_{h(q)}$. The generalized Hurst exponent of an image represents the local non-stationary property of the image. The initial window is shown in Fig. 2, the window slides from the left to right and top to bottom on each pixel in the image, then $L_{h(q)}$ of each pixel is obtained. In our task, the generalized Hurst exponents are obtained from the whole image, therefore, v is selected as 256. It is suggested that the minimum segment scale s should be larger than the polynomial fitting order k [9,20]. We assume minimum segment scale $s_{min} = 10$ and the maximum segment scale $s_{max} = 100$ for this case, and the

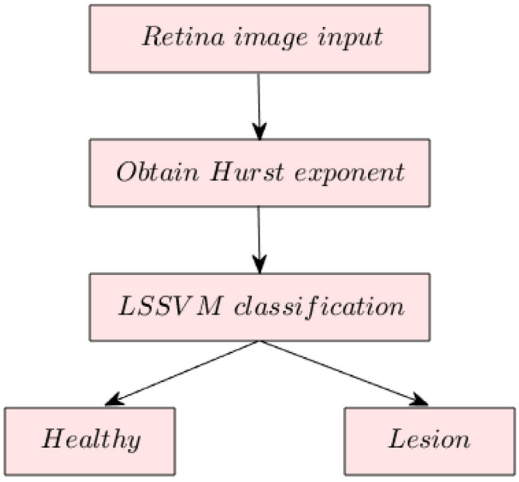

Fig. 1. Classification process of MF-DFA-LSSVM system.

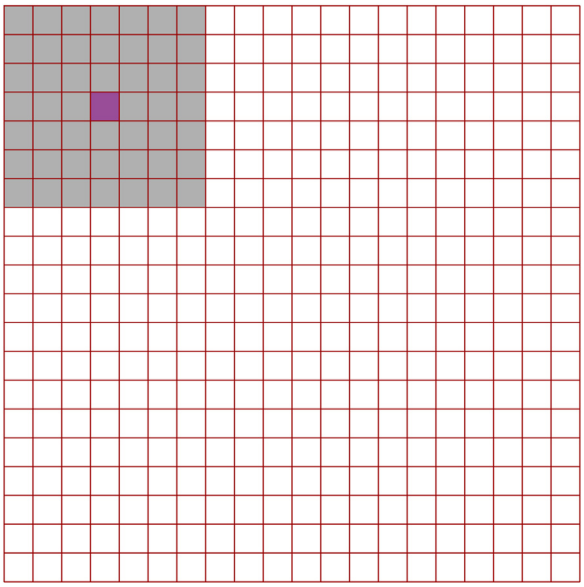

Fig. 2. Sliding window with size of 7 × 7.

segment size in total is chosen as 10. By [21,22], the fractal order q taken by $-10, -8, \ldots, 8, 10$ is enough.

2.2. 2D MF-DFA based image segmentation algorithm

The algorithm is based on the multifractal segmentation method. Each image can be regarded as a two-dimensional matrix gray levels. We calculate $L_{h(q)}$ for these images by the above algorithm. Firstly, we use a $v \times v$ window to traverse the whole image, the generalized $L_{h(q)}$ is calculated for each pixel point (i, j) according to the algorithm. We find the maximum and minimum values of the $L_{h(q)}$ of all pixels, and construct them into an interval $[L_{h(q_{\min})}, L_{h(q_{\max})}]$.

Then, we divide the interval into n equal segments. In each segment, we use the box counting method to calculate the fractal dimension of a sub-image composed of specific $L_{h(q)}$, which belongs to that segment. Then, a series of fractal dimensions can be obtained and expressed as $d_1(L_{h(q)}), d_2(L_{h(q)}), \ldots, d_n(L_{h(q)})$. We use $n = 30$ for the following tests.

The size of the moving window can significantly affect the accuracy of the algorithm; if the window is too large, then details will be missing, on the contrary, there are not enough points to fit the curve. For images with different pixels, we choose different window size $v \times v$, scale s in each window. According to [19], in this article, $v = 11$ and s ranges from 2 to 5.

In each segment, a box dimension is used to calculate the image consisting of $L_{h(q)}$, that is a sub-image which is composed of the $L_{h(q)}$ in an interval $[L_{h(q_{\min})}, L_{h(q_{\max})}]$. Then, a box of size $\alpha \times \alpha$ is used to cover a region in the sub-image, then we record the number in one box if $L_{h(q)}$ belongs to the interval. When the box slides over all the sub-image, we can get the number of boxes recorded as $N(\alpha)$. By changing the size of $\alpha \times \alpha$, a series of $N(\alpha)$ can be calculated by the power law

$$N(\alpha) = \left(\frac{1}{\alpha}\right)^{-d}. \tag{7}$$

then the spectrum $d(L_{h(q)})$ of MF-DFA can be defined by the gradient of the fitting line of the $N(\alpha)$ versus α.

As suggested by [19], here, we take $\alpha = 2, 4, 8, 16$, and 32. $d(L_{h(q)})$ represents the global singularity information of the image. The singularity of the image can be determined according to the value of $d(L_{h(q)})$ and it can be used as the segmentation criterion to segment the image. By judging the numerical results, the singularity of the image can be analyzed, and the appropriate range setting of $d(L_{h(q)})$ determines the singular region and the singular boundary of the image.

2.3. Least square support vector machine

The support vector machine, presented for classification and regression by Vapnik in 1995 [23], is a binary classification method. LSSVM is the least squares version of SVM and was developed by [25]. The difference between LSSVM and SVM is that LSSVM transforms the inequality constraints of the original method into equality constraints, and significantly facilitates the solution of Lagrange multipliers α which can be both positive or negative [26]. The original problem is a convex quadratic programming problem, while LSSVM is a problem of solving linear equations. Since LSSVM is actually solving linear equations, the calculation speed of LSSVM is obviously faster. Kernel function is a significant part of LSSVM, which enables the LSSVM to classify targets nonlinearly. For nonlinear classification, we need to find a mapping $\phi(\cdot)$ to map the original input data into a separation hyperplane and then maximize the objective function of the dual problem. The optimization problem of LSSVM is

$$minJ(\omega, e) = \frac{1}{2}||\omega||^2 + \frac{1}{2}\gamma\sum_{k=1}^{N} e_k^2 \tag{8}$$

with the constraints

$$y_k\left[\omega^T\phi(x_k) + b\right] = 1 - e_k, k = 1, \ldots, N, \tag{9}$$

where γ is the regularization parameter, and e_k is the random errors. Adopt Lagrange multiplier method

$$L(\omega, b, e, \alpha) = J(\omega, e) - \sum_{k=1}^{N}\alpha_k\left\{y_k\left[\omega^T\phi(x_k) + b\right] - 1 + e_k\right\}, \tag{10}$$

where α_k respond to Lagrange multipliers. Partial derivatives with respect to each parameter and let them equal 0, then we have

$$\begin{cases} \dfrac{\partial L}{\partial \omega} = 0 \rightarrow \omega = \displaystyle\sum_{k=1}^{N}\alpha_k y_k \phi(x_k), \\ \dfrac{\partial L}{\partial b} = 0 \rightarrow \displaystyle\sum_{k=1}^{N}\alpha_k y_k = 0, \\ \dfrac{\partial L}{\partial e_k} = 0 \rightarrow \alpha_k = \gamma e_k, k = 1, \ldots, N, \\ \dfrac{\partial L}{\partial \alpha_k} = 0 \rightarrow y_k[\omega^T\phi(x_k) + b] - 1 + e_k = 0, k = 1, \ldots, N. \end{cases} \tag{11}$$

Next, according to these four conditions, a system of linear equations for α and b can be formulated as

$$\begin{bmatrix} 0 & y^T \\ y & \Omega + I/\gamma \end{bmatrix}\begin{bmatrix} b \\ \alpha \end{bmatrix} = \begin{bmatrix} 0 \\ 1_v \end{bmatrix}, \tag{12}$$

where the element of Ω is $\Omega_{kl} = \phi(x_k)^T\phi(x_l) = K(x_k, x_l)$, $k, l = 1, \ldots, N$. $K(x_k, x_l)$ is the Gaussian kernel function and expressed by

$$K(x_i, x_j) = e^{-\frac{||x_k - x_l||^2}{2\sigma^2}}, \tag{13}$$

finally, LSSVM classification model is obtained by

$$y(x) = sign\left[\sum_{k=1}^{N}\alpha_k y_k K(x_k, x_l) + b\right], \tag{14}$$

where b is a bias. The LSSVM implementation is performed with MATLAB using the LS-SVMlab v1.8 toolbox available at: https://www.esat.kuleuven.be/sista/lssvmlab/. The parameters γ and σ^2 used in LSSVM should be appropriately selected to achieve the desired performance. After we have trained LSSVM with different combinations of γ and σ^2, we achieved the best result when $\gamma = 1$ and $\sigma^2 = 10$. The parameter tuning was guided by [24]. We use the leave-one-out cross-validation method for experimental verification. For evaluating the performance of the MF-DFA-LSSVM system, we calculated the mean and standard deviation for three evaluation metrics such as accuracy rate, sensitivity and specificity, and compared them with the state-of-arts.

2.4. LOOCV and performance evaluation

We adopt the LOOCV method for classification experiments by using LSSVM. The specific steps are as follows:

Step1: Randomly divide the Hurst exponents dataset for 130 real human retina images into k mutually exclusive subsets.
Step2: Randomly divide The k subsets into $k-1$ subsets and the other subset, thus, there are k partitioning methods in total.
Step3: In each group, the group of $k-1$ subsets are regarded as training set and the other as test set. Thus, k-times predictions are generated. Calculate the total accuracy of k-times predictions.
Step4: In order to ensure randomness, we repeat the above process P times. Therefore, it is called the P-times k-fold leave-one-out cross-validation method.

In this study, we take $P = 100$ and $k = 10$. Moreover, to evaluate the superiority of the proposed algorithm, we calculate the metrics such as the accuracy, sensitivity and specificity for the performance evaluation of classification. The three metrics are defined as follows.

$$Accuracy = \frac{TP + TN}{TP + FN + FP + TN}, \tag{15}$$

$$Sensitivity = \frac{TP}{TP + FN}, \tag{16}$$

$$Specificity = \frac{TN}{FP + TN}, \tag{17}$$

where TP, FN, TN, and FP denote $TruePositive$, $FalseNegative$, $TrueNegative$, and $FalsePositive$, respectively.

TP: An image is detected as lesion that is tagged as lesion.
FN: An image is detected as healthy that is tagged as lesion.
TN: An image is detected as healthy that is tagged as healthy.
FP: An image is detected as lesion that is tagged as healthy.

Accuracy is a statistical measure of the correct recognition of classifiers. Sensitivity is known as a true positive rate, which is described as the probability of getting a positive test result in subjects with the lesion. A greater sensitivity value implies that the diagnostic test is more sensitive. Specificity is expressed as a true negative rate, estimating the probability of getting a negative test result in a healthy subject. A greater specificity value indicates that the diagnostic test is more accurate [27]. Thus, all the three metrics can represent the ability of a diagnostic process to detect the lesion fundus images.

3. Data collection

The dataset of human retina images is selected from an open standard diabetic retinopathy database. The database contains 130 fundus images, of which 20 are healthy fundus images and the rest 110 are diabetic retinopathy images of varying degrees. For more information about the diabetic retinopathy database, please refer to "http://www.it.lut.fi/project/imageret/diaretdb0". We chose 130 images with 20 healthy and 110 lesion retina images. The samples of these images are all of calibration level 0, and with size of 1500×1152. The lesion retina images cover the images of diabetic retinopathy in different degrees, and each one has typical representative diabetic retinopathy tissue and shape. Four typical images of healthy and lesion images were selected and listed in Fig. 3(a) and Fig. 3(b), respectively.

As the first step, we transferred the original image to a two-dimensional gray image. The gray images of the first images in Fig. 3(a) and (b) are shown in Fig. 4.

4. Experiment results

We performed classification experiments with human retina images to show the robustness and efficiency of our proposed method. All the computations in this paper were computed by using Matlab R2018a on an Intel(R) Core(TM) i5-4430 CPU @ 3.00GHz processor. We analyzed multifractal features and local generalized Hurst exponents of the above two retina images in Fig. 4. The lesion image affected by the diabetic retinopathy leads to sharp changes in the local gray level. When calculating the local generalized Hurst exponents, we need to decide the parameters such as segment scale s and fractal order q. Because the image pixels in the diabetic retinopathy database were too large, we scaled the image pixels to the size of 256×256.

Before the multifractal analysis and classification of retina images, we first demonstrate whether our method can be applied for the automatic segmentation of retina images. The segmentation method is described in detail in Section 2.2. We take the original retina image of segmentation process as the same as Fig. 4(b), and the automatic segmentation results of lesion in retinal image are shown in Fig. 5. The performance depends on the interval of $d(L_{h(q)})$. After comparing the segmentation results of different intervals, the appropriate interval is selected as [2.25, 2.28].

The bleeding spots in the retinal image of diabetics are marked by boxes in Fig. 5(a), and the corresponding regions are segmented in Fig. 5(b). It can be seen that MF-DFA can effectively extract the features of the retina images. Therefore, we have reason to believe that the generalized Hurst exponents that obtained by MF-DFA method can be used to classify the fundus retina images.

To find whether there exists a linear relationship between the double-log plots of s and $F(q, s)$ is the first step of multifractal analysis. As shown in Fig. 6, the log-log plots of fluctuation function versus q are plotted for $q = -10, -8, \ldots, 8, 10$. The decreasing slope with the increasing of q indicates that both images have multifractal characteristics. Fig. 6(a) and (b) refer to the healthy and diabetic retinopathy affected images, respectively.

MF-DFA can show multifractality, scale invariance, and correlation of images. To better distinguish healthy and lesion retina images, we calculated the local generalized Hurst exponents $L_{h(q)}$ versus q for each image, see Fig. 7. Here, we notice that for the two images, the Hurst exponent curves perform significantly different.

We calculated all the Hurst exponents for 20 healthy and 110 lesion images and these Hurst exponents were taken as the input training vector for the classification of LSSVM. The mesh plots of $L_h(q)$ for 20 healthy retina images and 110 diabetic retinopathy affected retina images are shown in Fig. 8. The input Hurst exponents responding to a class label 0 for the healthy retina images and responding to a class label 1 for the diabetic retinopathy affected retina images.

Next, we used the leave-one-out cross-validation method that is introduced in Section 2.4 for classification experiments by LSSVM. Moreover, we calculate the metrics such as the accuracy, sensitivity, and specificity to evaluate the classification performance. With the

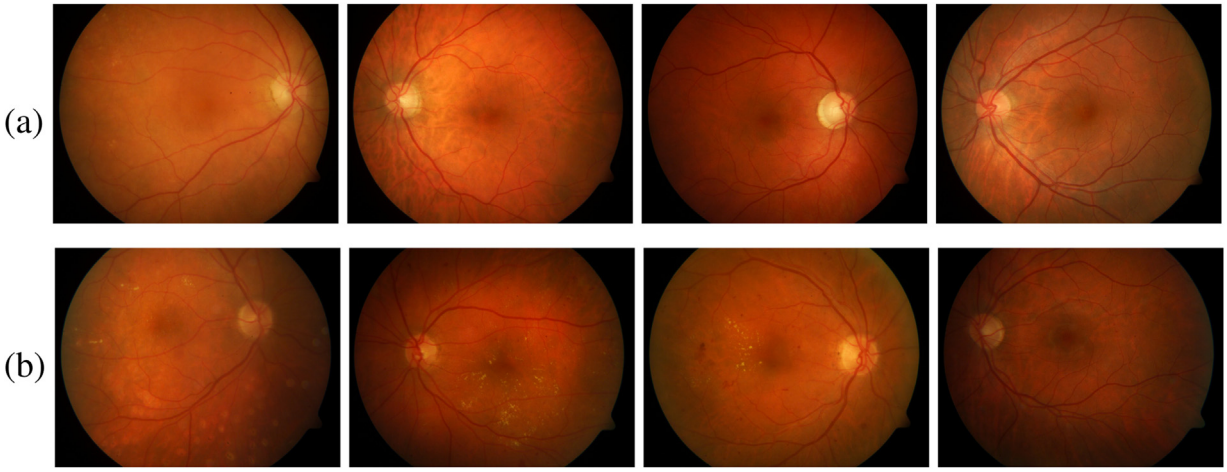

Fig. 3. Retina images of (a) healthy and (b) lesion.

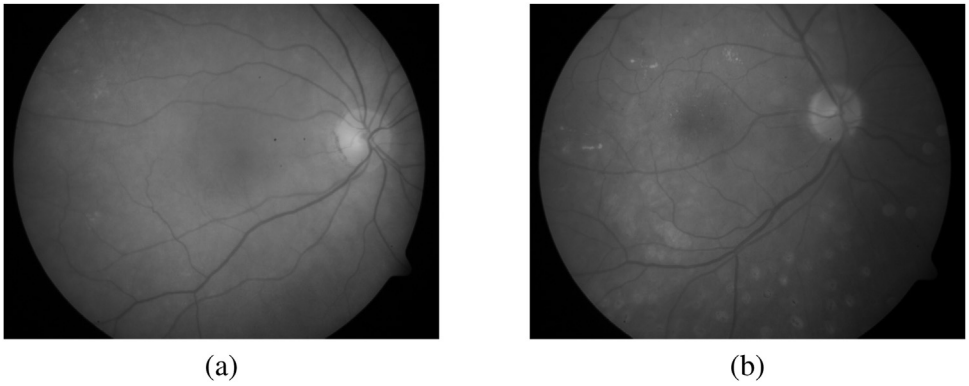

Fig. 4. Gray images of the first images in Fig. 3(a) and (b).

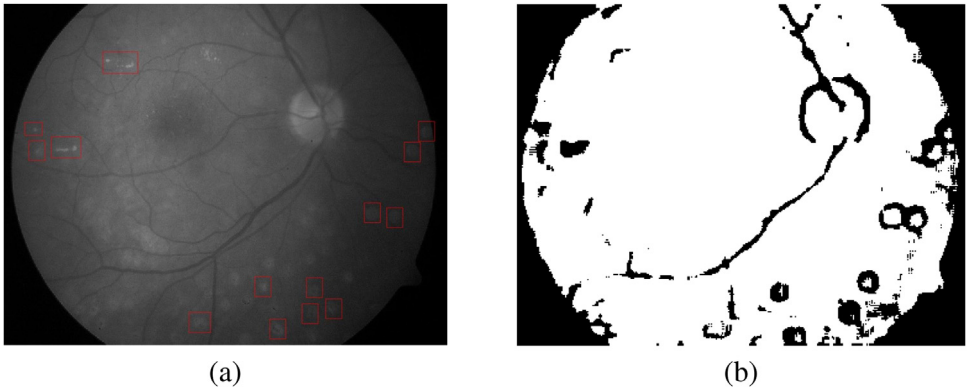

Fig. 5. Automatic segmentation process of (a) Original retina image and (b) segmented lesion regions.

classification of LSSVM, the obtained results of accuracy, sensitivity, and specificity versus iterations are shown in Fig. 9.

Using the above 100 random results of accuracy, sensitivity, and specificity, we averaged the data and calculated the standard deviation for three metrics. As shown in Table 1, the proposed MF-DFA-LSSVM system achieved 99.01% $\pm$ 0.0074 classification accuracy, 99.03% $\pm$ 0.0051 sensitivity, and 97.73% $\pm$ 0.0075 specificity. To better demonstrate the performance of the proposed system, we compared our method with some state-of-arts. The classification accuracy, sensitivity, and specificity of these methods are illustrated in Table 1. It can be observed from Table 1 that the proposed MF-DFA-LSSVM framework achieved the best performance in classification accuracy; the sensitivity and specificity are slightly less than [31,17], respectively. Generally, our system outperforms most of other methods in terms of all the classification of accuracy, sensitivity, and specificity.

5. Discussions

In this study, we used 130 fundus images from DIARETDB0 database to verify the efficiency and robustness of our proposed model which is composed by 2D MF-DFA and LSSVM. Based on the existing hybrid LSSVM classification methods for retina images, many methods achieved high classification accuracies. However, some models are complex and many steps are needed, the algorithms for classification are difficult to implement. It is worth

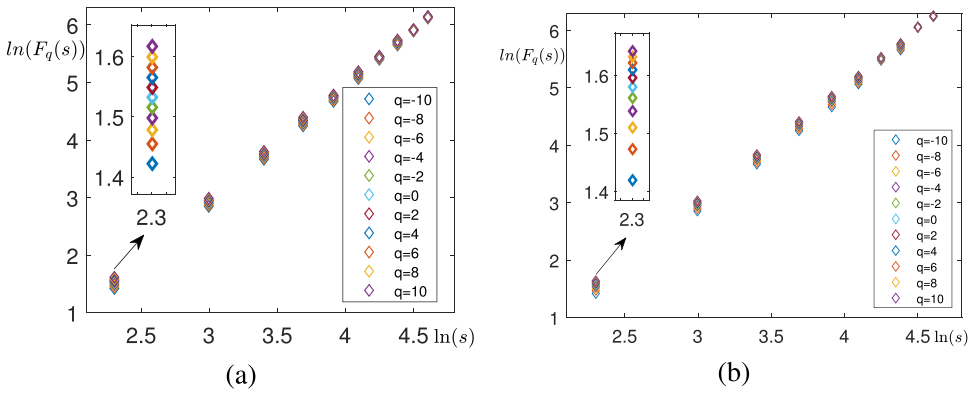

Fig. 6. Double logarithmic function diagram of (a) healthy and (b) diabetic retinopathy affected retina images. For interpretation of the references to color in this figure legend, the reader is referred to the web version of this article.

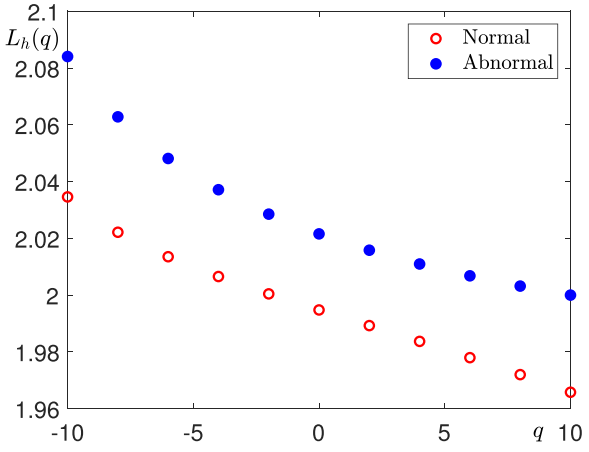

Fig. 7. Hurst exponents of healthy and lesion images.

mentioning that the proposed classification system in this paper only adopts Hurst exponents as the input training data, which is simple to implement. On the other hand, the system obtained satisfactory classification accuracy. Therefore, it can be seen that it will be useful in classifying the mutations in biological tissues of pathological patterns based on multifractal properties.

6. Conclusions

In this paper, the 2D MF-DFA-LSSVM system is proved to be an efficient classifier for solving retina fundus images classification problem. The proposed method combined 2D MF-DFA and LSSVM,

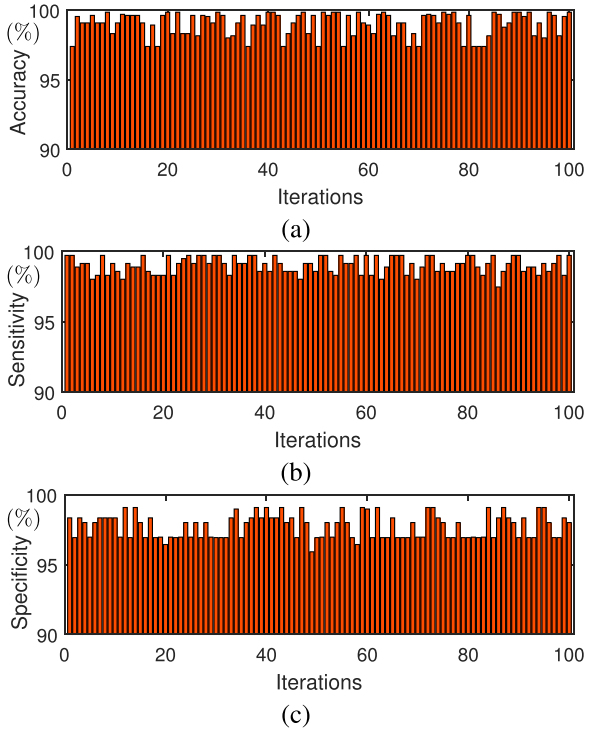

Fig. 9. Classification for dataset of 130 retina images with 100 random tests of (a) accuracy, (b) sensitivity, and (c) specificity.

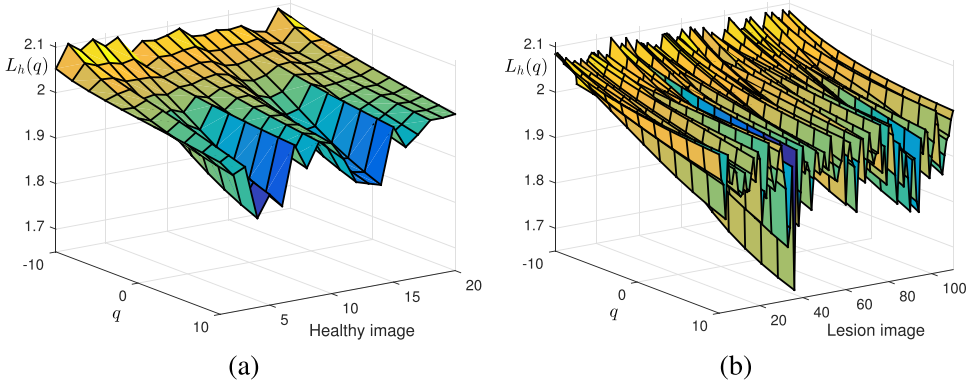

Fig. 8. Mesh plots of $L_h(q)$ of (a) healthy and (b) lesion.

Table 1
The comparison of obtained results with state-of-the-arts.

Task	Methods	Subjects number	Performance
Acharya [4]	Features from Gabor transform	510	*Accuracy* : 93.10% *Sensitivity* : 89.75% *Specificity* : 96.20%
Jadhav [16]	Morphological operation	89	*Accuracy* : 89.89% *Sensitivity* : 90.00% *Specificity* : 90.00%
Li [7]	Deep learning algorithm	48116	*Accuracy* : 98.6% *Sensitivity* : 95.6% *Specificity* : 92%
Pal [17]	Methodological approach	290	*Accuracy* : 98.55% *Sensitivity* : 98.74% *Specificity* : **98.55%**
Raghavendra [5]	Radon+MCT+ GIST+LSDA	1000	*Accuracy* : 97.00% *Sensitivity* : 97.80% *Specificity* : 95.80%
Koh [28]	Continuous wavelet transform	910	*Accuracy* : 92.48% *Sensitivity* : 89.37% *Specificity* : 95.58%
Omar [29]	Multiscale LBP texture	130	*Accuracy* : 98.68% *Sensitivity* : 94.81% *Specificity* : 96.73%
Prasad [30]	Haar wavelet transformations	89	*Accuracy* : 97.8% *Sensitivity* : 97.5% *Specificity* : 97.75%
Noronha [31]	Higher order spectra	272	*Accuracy* : 92.65% *Sensitivity* : **100%** *Specificity* : 92%
Giraddi [32]	Haar wavelet and First order statistical features	130	*Accuracy* : 85% *Sensitivity* : 87% *Specificity* : 80%
Maheshwari [6]	VMD and entropy	488	*Accuracy* : 95.19% *Sensitivity* : 93.62% *Specificity* : 96.71%
Raghavendra [8]	Eighteen layer CNN	1426	*Accuracy* : 98.13% *Sensitivity* : 98.00% *Specificity* : 98.30%
Stevenson [18]	Artificial intelligence algorithms	4435	*Accuracy* : 89.00% *Sensitivity* : 75.00% *Specificity* : 89.00%
Ours	2D MF-DFA-LSSVM	130	*Accuracy* : **99.01%** *Sensitivity* : 99.03% *Specificity* : 97.73%

and the local generalized Hurst exponents are computed by 2D MF-DFA. These Hurst exponents are given as the training feature input vector. Through the training of the LSSVM with the input vector, we classified specific retina fundus images as healthy or lesion retina images. We used the leave-one-out cross-validation method for experimental verification to investigate whether the created ensemble classifier (MF-DFA-LSSVM) with better accuracy for lesion retina detection. The MF-DFA-LSSVM system achieved classification accuracy, sensitivity, and specificity with a high satisfaction of $99.01\% \pm 0.0074$, $99.03\% \pm 0.0051$, and $97.73\% \pm 0.0075$, respectively. The empirical results demonstrated our method is superior to the other eight methods in three evaluation indicators. We concluded that the proposed method may be a promising system for clinic.

Author contributions

J.W. conceived the project and supervised all experiments. J.K. provided source code of the proposed method. W.S. searched for the sample, and performed all the figures and computational experiments. J.K., J.W., and W.S. wrote the manuscript. All authors read and edited the manuscript.

Acknowledgment

The first author (Jian Wang) was supported by the China Scholarship Council (201808260026). The corresponding author (J.S. Kim) expresses thanks for the support from the BK21 PLUS program. The authors greatly appreciate the reviewers for their constructive comments and suggestions, which have improved the quality of this paper.

Declaration of Competing Interest

The authors declare that they have no known competing financial interests or personal relationships that could have appeared to influence the work reported in this paper.

References

[1] Y. Horikawa, A. Suzuki, M. Enya, K.I. Hashimoto, S. Nishida, R. Kobayashi, M. Yamamoto, Periodontal disease may be associated with the occurrence of diabetic retinopathy: a subgroup analysis of the survey of the diabetes coordination notebook in gifu, Exp. Clin. Endocr. Diab. (2019).
[2] N. Thakur, M. Juneja, Survey on segmentation and classification approaches of optic cup and optic disc for diagnosis of glaucoma, Biomed. Signal Process. Control 42 (2018) 162–189.
[3] S.K. Saha, D. Xiao, A. Bhuiyan, T.Y. Wong, Y. Kanagasingam, Color fundus image registration techniques and applications for automated analysis of diabetic retinopathy progression: a review, Biomed. Signal Process. Control 47 (2019) 288–302.
[4] U.R. Acharya, E.Y.K. Ng, L.W.J. Eugene, K.P. Noronha, L.C. Min, K.P. Nayak, S.V. Bhandary, Decision support system for the glaucoma using Gabor transformation, Biomed. Signal Process. Control 15 (2015) 18–26.
[5] U. Raghavendra, S.V. Bhandary, A. Gudigar, U.R. Acharya, Novel expert system for glaucoma identification using non-parametric spatial envelope energy spectrum with fundus images, Biocyberne. Biomed. Eng. 38 (1) (2018) 170–180.
[6] S. Maheshwari, R.B. Pachori, V. Kanhangad, S.V. Bhandary, U.R. Acharya, Iterative variational mode decomposition based automated detection of glaucoma using fundus images, Comput. Biol. Med. 88 (2017) 142–149.
[7] Z. Li, Y. He, S. Keel, W. Meng, R.T. Chang, M. He, Efficacy of a deep learning system for detecting glaucomatous optic neuropathy based on color fundus photographs, Ophthalmology 125 (8) (2018) 1199–1206.
[8] U. Raghavendra, H. Fujita, S.V. Bhandary, A. Gudigar, J.H. Tan, U.R. Acharya, Deep convolution neural network for accurate diagnosis of glaucoma using digital fundus images, Inform. Sci. 441 (2018) 41–49.
[9] J.W. Kantelhardt, S.A. Zschiegner, E. Koscielny-Bunde, Multifractal detrended fluctuation analysis of nonstationary time series, Physica A 316 (1) (2002) 87–114.
[10] S. Lahmiri, S. Bekiros, Chaos, randomness and multi-fractality in Bitcoin market, Chaos Soliton. Fract. 106 (2018) 28–34.
[11] J. Wang, W. Shao, J. Kim, Cross-correlations between bacterial foodborne diseases and meteorological factors based on MF-DCCA: A case in South Korea, Fractals (2020), http://dx.doi.org/10.1142/S0218348X20500462.
[12] W. Shao, J. Wang, Does the "ice-breaking" of South and North Korea affect the South Korean financial market? Chaos Soliton. Fract. 132 (2020) 109564.
[13] S. Lahmiri, Multifractal analysis of Moroccan family business stock returns, Physica A 486 (2017) 183–191.
[14] G.F. Gu, W.X. Zhou, Detrended fluctuation analysis for fractals and multifractals in higher dimensions, Phys. Rev. E 74 (6) (2006) 061104.
[15] F. Wang, Q. Fan, H.E. Stanley, Multiscale multifractal detrended-fluctuation analysis of two-dimensional surfaces, Phys. Rev. E 93 (4) (2016) 042213.
[16] A.S. Jadhav, B.P. Pushpa, Classification of diabetes retina images using blood vessel area, IJCI 4 (2015).
[17] S. Pal, S. Chatterjee, Mathematical morphology aided optic disk segmentation from retinal images, in: 2017 3rd International Conference on Condition Assessment Techniques in Electrical Systems (CATCON), IEEE, Rupnagar, India, 2017, pp. 380–385.
[18] C.H. Stevenson, S.C. Hong, K.C. Ogbuehi, Development of an artificial intelligence system to classify pathology and clinical features on retinal fundus images, Clin. Exp. Ophthalmol. 47 (4) (2019) 484–489.
[19] Y. Yu, F. Wang, L. Liu, Magnetic resonance image segmentation using multifractal techniques, Appl. Surf. Sci. 356 (2015) 266–272.
[20] E.A.F. Ihlen, Introduction to multifractal detrended fluctuation analysis in Matlab, Fractal. Anal. Stat. Methodol. Innovations Best Pract. 97 (2012).
[21] B. Lashermes, P. Abry, P. Chainais, New insights into the estimation of scaling exponents, Int. J. Wavelets Multiresolut. Inf. Process. 2 (04) (2004) 497–523.
[22] F. Wang, Z.S. Li, J.W. Li, Local multifractal detrended fluctuation analysis for non-stationary image's texture segmentation, Appl. Surf. Sci. 322 (2014) 116–125.

[23] V. Vapnik, The Nature of Statistical Learning Theory, Springer-Verlag, New York, 1995.
[24] K. De Brabanter, P. Karsmakers, F. Ojeda, C. Alzate, J. De Brabanter, K. Pelckmans, J.A. Suykens, LS-SVMlab Toolbox User's Guide: version 1. 7, Katholieke Universiteit Leuven, 2010.
[25] J.A.K. Suykens, J. Vandewalle, Least squares support vector machine classifiers, Neural Process. Lett. 9 (3) (1999) 293–300.
[26] D. Tsujinishi, S. Abe, Fuzzy least squares support vector machines for multi-class problems, Neural Netw. Field 16 (2003) 785–792.
[27] P. Eusebi, Diagnostic accuracy measures, Cerebrovasc. Dis. 36 (4) (2013) 267–272.
[28] J.E. Koh, U.R. Acharya, Y. Hagiwara, U. Raghavendra, J.H. Tan, S.V. Sree, A. Laude, Diagnosis of retinal health in digital fundus images using continuous wavelet transform (CWT) and entropies, Comput. Biol. Med. 84 (2017) 89–97.
[29] M. Omar, F. Khelifi, M.A. Tahir, Detection and classification of retinal fundus images exudates using region based multiscale LBP texture approach, 2016 International Conference on Control, Decision and Information Technologies (CoDIT) (2016) 227–232.
[30] D.K. Prasad, L. Vibha, K.R. Venugopal, Early detection of diabetic retinopathy from digital retinal fundus images, 2015 IEEE Recent Advances in Intelligent Computational Systems (RAICS) (2015) 240–245.
[31] K.P. Noronha, U.R. Acharya, K.P. Nayak, R.J. Martis, S.V. Bhandary, Automated classification of glaucoma stages using higher order cumulant features, Biomed. Signal Process. Control 10 (2014) 174–183.
[32] S. Giraddi, S. Gadwal, J. Pujari, Abnormality detection in retinal images using Haar wavelet and First order features, 2016 2nd International Conference on Applied and Theoretical Computing and Communication Technology (iCATccT) (2016) 657–661.